


Enhanced condensation heat transfer by water/ethanol binary liquids on polydimethylsiloxane brushes

Shuai Li¹ | Diego Diaz¹ | Michael Kappl¹ | Hans-Jürgen Butt¹  | Jie Liu^{1,2,3} | Youmin Hou^{1,4}

¹Physics at Interfaces, Max Planck Institute for Polymer Research, Mainz, Germany

²Key Laboratory of Green Printing, Institute of Chemistry, Chinese Academy of Sciences, Beijing, China

³School of Chemical Sciences, University of Chinese Academy of Sciences, Beijing, China

⁴School of Power and Mechanical Engineering, Wuhan University, Wuhan, China

Correspondence

Hans-Jürgen Butt, Physics at Interfaces, Max Planck Institute for Polymer Research, Ackermannweg 10, 55128 Mainz, Germany. Email: butt@mpip-mainz.mpg.de

Jie Liu, Key Laboratory of Green Printing, Institute of Chemistry, Chinese Academy of Sciences, Beijing 100190, China; School of Chemical Sciences, University of Chinese Academy of Sciences, Beijing 100049, China. Email: liujie123@iccas.ac.cn

Youmin Hou, School of Power and Mechanical Engineering, Wuhan University, Wuhan 430072, China. Email: houyoumin@whu.edu.cn

Funding information

H2020 European Research Council, Grant/Award Number: 883631

Abstract

Enhancing heat transfer efficiency by liquid condensation plays a critical role in recovering and utilizing low-grade heat. However, overall heat transfer efficiency is commonly limited by the inefficient vapor–liquid phase transition flux and enthalpy during liquid condensation. Here, we report that by introducing small amount of water into the phase-change process of ethanol on a liquid-like polydimethylsiloxane (PDMS) brush surface, the heat transfer coefficient is significantly enhanced, in particular, by more than one order of magnitude compared to the pure ethanol condensation. Such enhanced thermal performance is primarily due to the elaborate balance between promoting condensation, that is, nucleation and growth, and increasing latent heat by regulating components of water and ethanol, as well as the rapid droplet removal by condensing on the PDMS brushes. Note that the more stabilized dropwise condensation of the binary liquids, retained by accelerating the droplet coalescence velocity, beyond filmwise condensation ensures its significant effectivity under high heat flux.

INTRODUCTION

Vapor condensation is a ubiquitous phenomenon in nature and also an essential process in many industrial applications, for example, heat pipes,^{1,2} air conditioning,^{3,4} and power generation.⁵ Enhancing the condensation performance of liquids would significantly improve the overall thermal efficiency, leading to global energy savings. Dropwise condensation on a solid surface, during which discrete mobile droplets form and are easily shed from the surface by gravity, is a favorable way to improve heat transfer efficiency.^{6–8} To

accelerate such a process, a high vapor–liquid phase transition flux on solid surfaces is required, which is commonly achieved by promoting droplet nucleation, growth, and departure (Figure 1). The rapid droplet departure promotes the overall heat transfer rate by reducing the thermal barrier associated with the condensate and clearing the surface for droplet renucleation.^{9,10} Besides that, reducing the surface tension of liquids is an efficient approach commonly used to promote condensation.^{11–16} However, the condensation of low-surface-tension liquids is typically characterized by the formation of a liquid film that entirely covers the condensing

This is an open access article under the terms of the Creative Commons Attribution License, which permits use, distribution and reproduction in any medium, provided the original work is properly cited.

© 2022 The Authors. *Droplet* published by Jilin University and John Wiley & Sons Australia, Ltd.

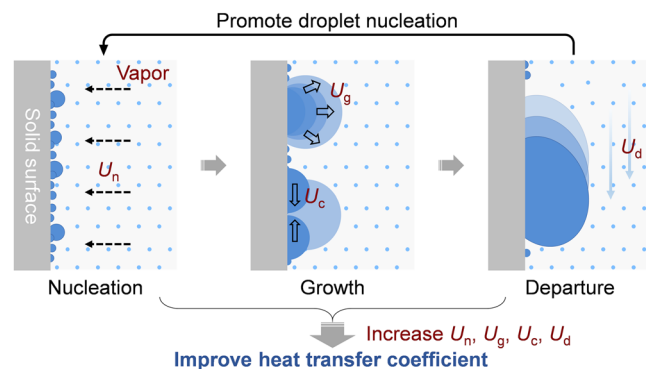


FIGURE 1 Overview of factors promoting the heat transfer coefficient. U_n , U_g , U_c , and U_d represent the rate of liquid nucleation, growth, coalescence, and departure on a solid surface.

surface since these liquids wet most solid materials with a low contact angle. The liquid film results in high thermal resistance and slows the condensate departure, thereby decreasing the heat transfer coefficient.

In recent years, intensive research has focused on developing advanced omniphobic materials, such as lubricant-infused surfaces^{17–19} and flexible polymer brush coatings,^{20–22} on which dropwise condensation of various liquids is demonstrated. For the common low-surface-tension liquids (e.g., ethanol, hexane, and toluene), the thermal performances of dropwise condensation on omniphobic surfaces are superior to those of filmwise condensation. However, efficient heat transfer requires not only rapid droplet nucleation and departure but also a high enthalpy of condensation (i.e., latent heat of vaporization). For low-surface-tension liquids, the low latent heat of vaporization and thermal conductivity greatly limit the thermal performance of phase change (Supporting Information: Figure S1). The condensation heat transfer coefficient of ethanol, a representative low-surface-tension liquid (with surface tension γ_{lv} of 22.8 mN m^{-1}), was only $10\text{--}20 \text{ kW m}^{-2} \text{ K}^{-1}$, as much as $30\text{--}70\%$ lower than that of pure water.^{16,18,20} Therefore, displaying high vapor–liquid phase transition flux and stable dropwise condensation on a solid surface while balancing the vaporization latent heat are dominant for improving heat transfer efficiency.

In this study, we report a significant heat transfer enhancement by introducing a small portion of water into the condensation process of ethanol on an omniphobic polydimethylsiloxane (PDMS) brush surface. The binary liquids increased the latent heat without diminishing the low-surface-tension properties of the condensate, therefore gaining the advantages of high nucleation density, fast growth rate, and rapid droplet shedding. In addition, the binary liquids accelerated the relaxation of coalescing droplets, which effectively stabilized the dropwise condensation under high heat flux. As a result, the binary condensation of ethanol–water mixtures achieved an 1800% higher heat transfer coefficient on the PDMS brush surface when compared with the ethanol condensation. Our experimental results reveal a previously unnoticed correlation between droplet coalescence hydrodynamics and the optimal thermal performance of low-surface-tension

liquids, which can shed more light on the phase change process and associated heat transfer applications.

RESULTS AND DISCUSSION

When condensing the mixture of water and ethanol on the solid surface (Figure 2a), the ethanol concentration in the binary liquids determines the thermophysical properties and influences the heat and mass transfer rate during binary condensation. Figure 2b plots the variation of surface tension, nucleation energy barrier, and latent heat of vaporization for the condensate against the volume fraction of ethanol ϕ_e in the binary condensate. We measured the surface tension of the binary condensate with a DataPhysics tensiometer and estimated the nucleation energy barrier of binary liquids using the classical nucleation theory (see theoretical calculation in the Supporting Information).^{9,23–25} The increased ϕ_e reduced the liquid surface tension and the nucleation energy barrier, which enhanced the nucleation rate in the condensation process. However, the trade-off for the nucleation enhancement of binary liquids was the reduction in latent heat of vaporization. This conflict implies that the efficient heat transfer of binary condensation necessitates sensitive tuning of the ethanol concentration to achieve the optimal balance between the enhanced nucleation and the high latent heat of vaporization. For convenient description here, BL-70, BL-80, and BL-90 are used to denote the binary liquids with $\phi_e = 70\%$, 80% , and 90% , respectively.

To decrease the interfacial thermal resistance of the condensate, we used an omniphobic surface coated with PDMS brushes (Figure 2c) to ensure the dropwise condensation of binary liquids.^{23,26} The PDMS brushes consist of polymer chains of repeating siloxane groups ($-\text{O}-\text{Si}(\text{CH}_3)_2-\text{O}-$), which were covalently grafted onto a silicon substrate. To prepare the PDMS brushes, the O_2 plasma-treated silicon substrates were immersed in water-saturated toluene with dichlorodimethylsilane. After 30 min, the surface was uniformly coated by PDMS polymer brushes with a thickness of $\sim 4 \text{ nm}$. The prepared PDMS brushes exhibit great durability even after ultrasonic washing for 30 min (Supporting Information: Figure S2). Because of the high flexibility and low surface roughness of the siloxane chains (see AFM data in Supporting Information: Figure S3),^{27,28} the PDMS coating showed excellent repellency against the binary liquids with extremely low surface tension (see contact angle data in Table 1). All the binary liquids exhibited a contact angle hysteresis of less than 6° on the PDMS brushes (Supporting Information: Figure S4a). The low contact angle hysteresis results in a low lateral adhesion force F on the surface, which can be calculated by^{29–31}

$$F = kw\gamma(\cos\theta_R - \cos\theta_A), \quad (1)$$

where k , w , γ , θ_R , θ_A denote the dimensionless factor, droplet contact width, surface tension of the liquid, receding contact angle, and advancing contact angle, respectively.

As the surface tension and contact angle hysteresis determine the droplet adhesion force, the mobility of binary liquids on PDMS

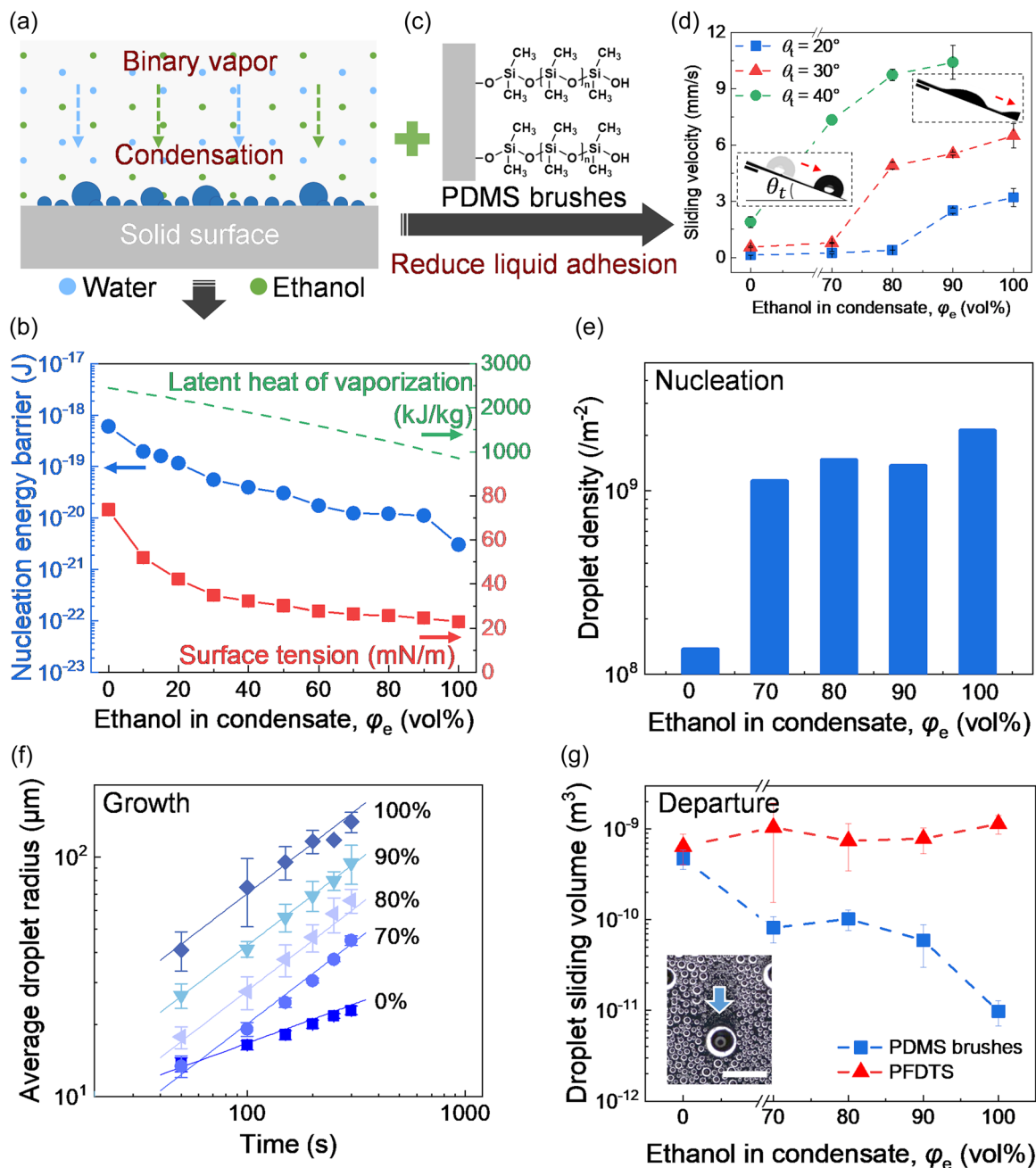


FIGURE 2 Condensation characterization. (a) Schematic of the binary condensation. (b) Nucleation energy barrier, surface tension, and latent heat of vaporization of ethanol–water mixtures as a function of ethanol concentration. Nucleation energy barrier was calculated based on the classical nucleation equation. (c) Schematic of the chemical structure of PDMS brushes. (d) Sliding velocity of droplets of ethanol–water mixtures on tilted ($\theta_t = 20^\circ, 30^\circ, 40^\circ$) PDMS brushes. Water: $5 \mu\text{L}$, others: $3 \mu\text{L}$. Room humidity: 30%. Inset: Sliding photographs of water and binary liquid ($\varphi_e = 90\%$) droplets on tilted ($\theta_t = 40^\circ$) PDMS brushes (Scale bar: 2 mm). θ_t refers to the tilt angle. (e) Initial nucleation site density of liquids on PDMS brushes. (f) Time evolution of the average droplet radius of various condensed liquids on PDMS brushes. The solid lines denote the droplet growth model $r = \beta t^\alpha$, where the slopes are the power law exponent α (0.3 for water and 0.7 for other low-surface-tension liquids). (g) Droplet departure volumes on the vertical PDMS brushes (blue symbols) and hydrophobic PFDTs surface (red symbols) as a function of ethanol concentration. Departure droplet sizes were estimated by comparing sequential images before and after departure during the condensation process. Inset: Image showing the departure of a water droplet on PDMS brushes (Scale bar: 2 mm). PDMS, polydimethylsiloxane; PFDTs, perfluorodecyltrichlorosilane.

brushes was enhanced by increasing φ_e (Figure 2d and Supporting Information: Figure S3B). Compared with pure water, BL-90 demonstrated $\sim 25\%$ less adhesion force, which was only $5.9 \mu\text{N}$. Therefore, a $3 \mu\text{L}$ droplet of BL-90 moved with an average velocity of

$\sim 10.5 \text{ mm s}^{-1}$ on the PDMS brushes with a tilted angle $\theta_t = 40^\circ$, which was approx. five times faster than that of a $5 \mu\text{L}$ water droplet (Supporting Information: Figure S5). We also measured the droplet mobility of binary liquids on the hydrophobic surface coated with

TABLE 1 Advancing contact angle and receding contact angle of binary liquids on PDMS brushes.

Ethanol in condensate, φ_e (vol%)	0	70	80	90	100
Advancing contact angle (°)	104 ± 1	52 ± 1	48 ± 1	45 ± 1	29 ± 2
Receding contact angle (°)	101 ± 1	46 ± 1	43 ± 1	39 ± 1	25 ± 2

1H, 1H, 2H, 2H-perfluorodecyltrichlorosilane (PFDTs). Although the surface energy of PFDTs coating was lower than PDMS brushes, the droplet of binary liquids showed a larger contact angle hysteresis (~25°) and higher lateral adhesion force (~30 μN) on the hydrophobic surface (Supporting Information: Figure S4b). These results suggest that the PDMS brushes favor the rapid transport of binary liquids, which can decrease the interfacial thermal resistance during binary condensation.

The condensation dynamics of binary liquids on the PDMS brushes were first characterized in a custom-made chamber coupled with optical microscopy (Supporting Information: Figure S6). Nitrogen gas flow carried the saturated binary vapor into the chamber with a stabilized flow rate at ~1 L min⁻¹. The surface temperature was adjusted using a Peltier element with circulating cooling water, and the subcooling between the saturated vapor and surface was maintained at ~10 K for the experiments here. The video of condensation was recorded by a camera (Ueye, UI-2240SE-C-HQ) for further analysis.

At the initial stage, the binary liquids condensed with high droplet number density due to the low nucleation energy barrier (Figure 2b,e and Supporting Information: S6A^{7,32,33}). At $t=0$ s (Figure 2e), the droplet density of BL-90 was $1.4 \times 10^9 \text{ m}^{-2}$, which was one order of magnitude higher than that of water. As condensation time increased, the number density of pure water droplets remained stable, whereas the density of the binary condensate decreased continuously (Supporting Information: Figure S7a, for example, for BL-90, it dropped to $3.6 \times 10^7 \text{ m}^{-2}$ at $t=300$ s). The considerable variation of droplet number density can be explained by the rapid droplet growth and frequent coalescence during binary condensation, which was also indicated by the time evolution of the droplet radius shown in Figure 2f. The average radius of condensing droplets follows the equation of $r = \beta t^\alpha$, where t is the condensation time and α is the power law exponent representing the droplet growth mechanism.^{34–36} During the first 300 s, α for the binary liquids was ~0.7 and for water was ~0.3. The small α for water condensation suggests that most of the water droplets grow independently without coalescence in the first 300 s.^{37,38} By contrast, the droplets of binary liquids coalesce much more frequently due to the narrow droplet spacing and small contact angle, thus leading to the rapid growing radius and large α in the droplet growth model.

Figure 2g shows the volume of sliding droplets on the condensing surface as a function of ethanol concentration φ_e in the binary liquids. For the omniphobic PDMS surface, the sliding

volume of condensing droplets decreased with increasing φ_e , which was consistent with the results of sessile droplet sliding tests (Figure 2d). The low lateral adhesion force enables BL-90 rapidly slide off the PDMS brushes at a volume of $6 \times 10^{-11} \text{ m}^3$, which was ~90% less than that of water. As a comparison, the droplet sliding volume on the hydrophobic PFDTs surface was independent of φ_e . Although the sliding volume of pure water droplets was comparable on both hydrophobic and omniphobic surfaces, the low-surface-tension binary liquids slid more efficiently on the PDMS brushes. The rapid liquid transport, therefore, reduces the interfacial thermal resistance associated with condensing droplets on the surface.

The measurements of droplet number density and radius enable us to estimate the condensation rate and heat flux during the first 300 s of the experiment (see details in Supporting Information: Figure S7). The results show that the condensation heat flux of binary liquids did not monotonically rise with the increasing ethanol concentration. Specifically, BL-90, rather than pure ethanol, showed the highest condensation rate. At $t=300$ s, the total condensate weight of BL-90 was $6.4 \times 10^{-9} \text{ kg}$, which was 35% higher than that of pure ethanol. Despite the extremely high nucleation density, pure ethanol is not ideal for achieving efficient condensation because the small contact angle limits the volume of individual droplets. This phenomenon indicates that the appropriate mix of water and ethanol is essential to enhance the condensation heat transfer, which should not rely solely on either the high latent heat of vaporization (e.g., water) or the increased nucleation rate (e.g., ethanol).

To accurately determine the heat transfer performance of binary condensation at a steady state, we tested the omniphobic PDMS brushes and the hydrophobic PFDTs surface in a custom-built condensation chamber, as shown in Figure 3a and Supporting Information: Figure S8. The sample was vertically mounted on a cooling stage to ensure continuous droplet sliding by gravity, and the surface temperature was controlled by circulating cooling water. Before the experiment, the chamber was evacuated to a pressure below 10 Pa to eliminate the influence of noncondensable gases on the condensation heat transfer.^{8,39} The vapor of binary liquids was generated in a boiler and then introduced into the chamber. The vapor and surface temperatures in the chamber were measured with Pt100 RTD sensors to determine the subcooling of the surface. The flow rates and temperatures of cooling water at the inlet and outlet of the cooling stage were measured to calculate the overall heat flux and condensation heat transfer coefficient on the surface.^{40–42} Through the viewport of the condensation chamber, the droplet morphology and departure rate were recorded via a camera with a macrolens.

The experimentally determined condensation heat transfer coefficient on the PDMS brushes and PFDTs surfaces is plotted as a function of φ_e in Figure 3b. Compared to pure water and ethanol, the condensation of binary liquids substantially enhances the heat transfer performance. BL-90 demonstrated the highest condensation heat transfer coefficient $h \approx 57 \text{ kW m}^{-2} \text{ K}^{-1}$ on the

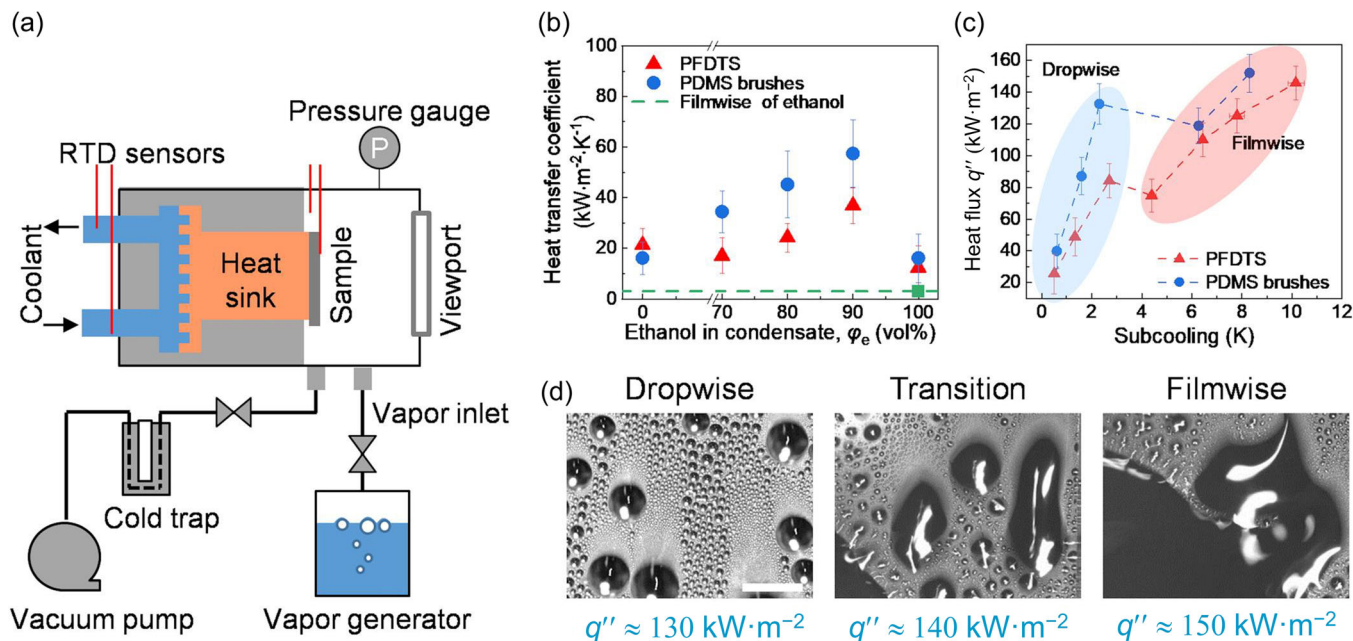


FIGURE 3 Enhanced heat transfer of binary condensation. (a) Schematic of the experimental setup for thermal characterization of binary condensation. (b) Condensation heat transfer coefficient of binary liquids on PDMS brushes and on the hydrophobic PFDTs surface at a subcooling of ~ 2 K. The green square and the dashed line denote the theoretical value of the heat transfer coefficient for filmwise ethanol condensation. (c) Condensation heat flux of binary liquids BL-90 as a function of subcooling on different surfaces. The areas shaded in blue and red denote the dropwise and filmwise condensation regimes. (d) Images showing the dropwise condensation, the transition from dropwise to filmwise condensation, and the filmwise condensation of BL-90 on PDMS brushes under different heat fluxes. Error bars were calculated from the uncertainties of specific heat capacity and density of water, temperature, flow rate, and surface area via error propagation (see the Supporting Information for details). PDMS, polydimethylsiloxane; PFDTs, perfluorodecyltrichlorosilane.

PDMS brushes. It was more than 1800% higher when compared to the filmwise condensation of ethanol (the green square and dashed line in Figure 3c, $h \approx 3 \text{ kW m}^{-2} \text{ K}^{-1}$) and 250% higher than that of water ($h \approx 16 \text{ kW m}^{-2} \text{ K}^{-1}$). For comparison, in a recent study, Nenad et al.¹⁹ achieved 200% enhancement in the condensation heat transfer coefficient with stable dropwise condensation of ethanol; they used tubes and impregnated their hydrophobic surfaces with Krytox 1525. Due to inefficient droplet shedding, the hydrophobic PFDTs surface showed a $\sim 35\%$ lower heat transfer coefficient than the omniphobic PDMS brushes in the same condensation environment. Nevertheless, the heat transfer coefficient of binary condensation on the hydrophobic surface was still $\sim 200\%$ higher than that of ethanol. These results confirmed that the introduction of a small amount of water into ethanol could, in fact, be a general strategy to improve the overall heat transfer performance during the condensation process.

We also investigated the effect of subcooling on condensation morphology to provide further insight into the optimal binary condensation heat transfer performance. Figure 3c demonstrates the variation of condensation heat flux for BL-90 with the increasing surface subcooling. We observed that dropwise condensation only prevailed when the condensation heat flux was below a critical value (Figure 3d and Supporting Information:

Figures S8–S9). The PDMS brushes sustained the dropwise binary condensation when the heat flux was below $\sim 130 \text{ kW m}^{-2}$. Once the heat flux exceeded the threshold, the condensate transitioned from the droplet morphology to a liquid film with an irregular shape (Figure 3d). When the heat flux increased to 150 kW m^{-2} , the liquid film expanded further and eventually merged to cover the whole surface. Accordingly, the condensation heat transfer coefficient decreased with increasing subcooling when filmwise condensation dominated (Figure 3c). The PDMS brushes demonstrated a significantly higher critical heat flux than the hydrophobic PFDTs surface in the same condensation environment. For BL-90, the critical heat flux on PDMS brushes was 60% higher than that on the PFDTs surface ($\sim 80 \text{ kW m}^{-2}$). Such enhanced critical heat flux on the PDMS brushes was also applicable to other binary liquids, for example, BL-70 and BL-80 (see Supporting Information: Figure S11 for more experimental data). These results demonstrate that the dropwise condensation morphology depends not only on the static contact angle of binary liquids but also on the other wetting characteristics and condensation rates on the surface.

The transition from dropwise to filmwise condensation for binary liquids can be understood as an incomplete relaxation of a coalesced droplet due to the increased coalescence frequency under high heat flux.^{43,44} As shown in Figure 4a, when two droplets

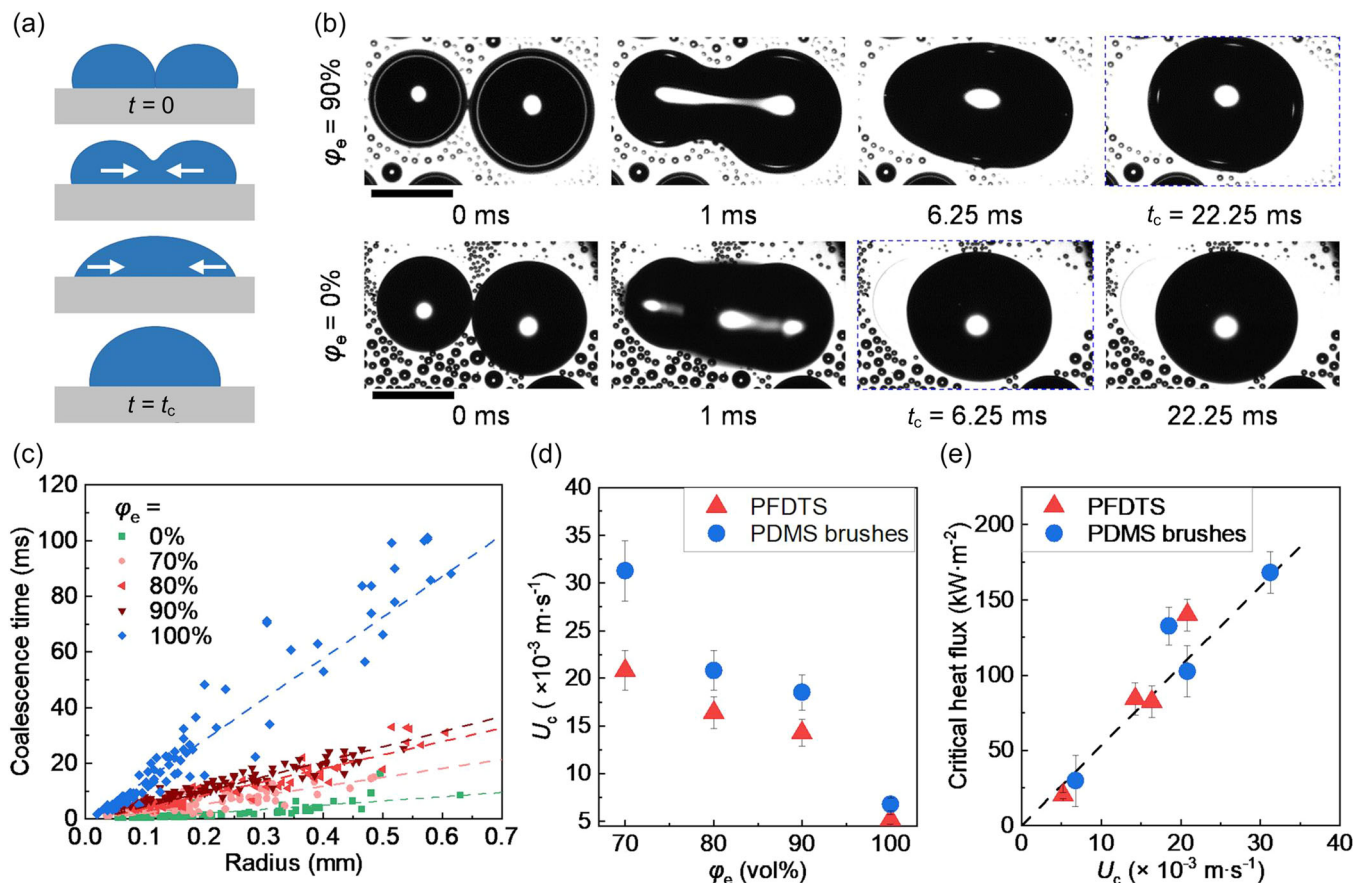


FIGURE 4 Droplet coalescence and critical heat flux during binary condensation. (a) Schematic showing the droplet coalescence process during condensation. t_c refers to the time scale of droplet coalescence, which is defined as the time period from the instant of two droplets getting into contact ($t = 0$) to the stabilization of the coalesced droplet ($t = t_c$). (b) Time-lapsed images showing the droplet coalescence of water and BL-90 ($\phi_e = 90\%$) on PDMS brushes. B rectangles highlight the time ($t = t_c$) when the droplets finish the coalescence processes (Scale bar: 0.5 mm). (c) Coalescence time t_c as a function of the droplet radius for different liquids on PDMS brushes. (d) Values of U_c (coalescence velocity) on PDMS brushes and hydrophobic surfaces as a function of ethanol concentration. (e) Experimental critical heat flux as a function of U_c on PDMS brushes and on a fluorinated surface. PDMS, polydimethylsiloxane; PFDTs, perfluorodecyltrichlorosilane.

contact each other by growth, it takes some time for the droplet to revert to a more spherical shape driven by the liquid surface tension. The time required for the coalesced droplet to relax to the equilibrium state was defined as the coalescence time, t_c .⁴⁵ If the coalescence frequency becomes so high that droplets do not have time to revert to their new equilibrium shape, the condensate would appear as a continuous liquid film rather than as discrete droplets on the surface.

To explore the effect of ϕ_e on the droplet coalescence hydrodynamics, we experimentally measured t_c for different condensing liquids on PDMS brushes by using a high-speed camera. As shown in Figure 4b and Supporting Information: Movie S1–S2, the binary liquids showed slower coalescence when compared to pure water. For the coalescence of two droplets with $r \approx 0.85$ mm on the PDMS brushes, the coalescence time t_c was 6 ms for water and 22 ms for BL-90. The low surface tension of binary liquids reduces the driving force for coalescence, thus slowing down the relaxation of the coalescing droplet.

When plotting the droplet coalescence time t_c for the binary liquids against the droplet radius r , we obtained a linear relationship between t_c and r for all liquids (Figure 4c). Based on the experimental results, a characteristic velocity U_c can be defined to characterize the coalescence velocity for different condensing liquids:

$$U_c = \frac{r}{t_c}. \quad (2)$$

Figure 4d shows the experimentally determined U_c of the condensing droplets with different ϕ_e on the PDMS brushes and the hydrophobic PFDTs surfaces. Our measurement of characteristic velocity for water droplet coalescence is faster than that reported by Beysens,⁴⁵ but agrees well with later observations.^{46,47} The measured U_c of binary liquids decreased with the increasing ϕ_e , which showed the opposite trend compared to the sliding velocity (Figure 1d). A substantial increase in droplet coalescence velocity U_c was observed when a small portion of water was added to ethanol. For BL-90, the corresponding $U_c \sim 1.9 \times 10^{-2} \text{ m}\cdot\text{s}^{-1}$ was $\sim 170\%$ higher

than that of pure ethanol on the PDMS brushes ($\sim 7 \times 10^{-3} \text{ m s}^{-1}$), therefore resulting in a much more stable dropwise condensation state as demonstrated by the experimental results (Figure 3d).

Droplet coalescence velocity U_c on the PDMS brushes was consistently higher than that on the hydrophobic PFDTs surface, with a difference of up to 50% when $\phi_e = 70\%$ (Figure 4d). The rapid droplet coalescence indicated that the liquid contact line moved with less resistance on the PDMS brushes due to the lower droplet adhesion force. Since the rapid droplet coalescence creates more surface area available for nucleation, we obtain a positive correlation between the critical condensation heat flux q''_{cr} and the coalescence velocity U_c (Figure 4e). Note that this positive correlation reveals no statistical difference between the PDMS brushes and the PFDTs surface, which underscores that it is the droplet coalescence hydrodynamics on the surface rather than the droplet departure ability that plays a defining role in stabilizing the dropwise condensation under high heat flux.

Our exploration of critical heat flux reveals that efficient binary condensation is due to the synergy of optimized liquid thermo-physical properties and liquid/solid interaction. The low contact angle hysteresis on PDMS brushes leads to rapid droplet sliding and high coalescence velocity of binary liquids, thus achieving a high heat transfer coefficient. Note that the enhanced heat transfer by binary condensation is not limited to the ethanol-water mixture. We anticipate that other binary liquids, for example, water/isopropanol, water/glycol, and so on, can also promote heat transfer when the latent heat and liquid surface tension are carefully adjusted. Future development could go a step further by implementing this strategy to the condensing surfaces with textures or gradient wettabilities,^{48–52} which may break the limit of heat transfer performance. Meanwhile, although the PDMS brushes show good durability after ultrasonic washing, the durability for sustaining dropwise condensation in the long term is still needed to be considered in the future. Additional techniques can be combined, for example, micro/nanostructures or inorganic coatings, to advance the approach to real-life applications.⁵³

CONCLUSION

This study successfully enhanced the condensation heat transfer by adding small amount of water during the phase-change process of ethanol. The condensation of binary liquids exhibited a high nucleation and growth rate while allowing for the rapid droplet departure. As a result, the binary condensation on the omniphobic PDMS brushes increased the heat transfer coefficient by more than 1800% compared to the filmwise ethanol condensation. Moreover, the binary liquids accelerated the droplet coalescence, thus effectively avoiding the filmwise condensation of low-surface-tension liquids under high heat flux. These results can help to fundamentally improve the phase-change heat transfer of liquids in a wide range of applications such as power generation, thermal management, and waste heat recovery.

METHODS

PDMS brushes: Silicon wafers (Silicon Materials Inc, P type, (1 0 0) orientation) were ultrasonicated in toluene (98%, Sigma) and ethanol (99.5%, Sigma) for 5 min and dried with nitrogen. Then, the substrates were cleaned with oxygen-plasma (Diener Electronic Femto, 120 W, $6 \text{ cm}^3 \text{ min}^{-1}$ oxygen flow rate) for 5 min and immersed in a mixture of 40 mL of toluene (with saturated water) and 1.4 mL of dimethyldichlorosilane. After 0.5 h, the substrate was taken out, washed with toluene, and dried with nitrogen.

Fluorinated surface: Silicon wafers were washed ultrasonically for 5 min with toluene and ethanol, as described above. Afterward, wafers were treated with 120 W oxygen-plasma for 5 min before being placed into a vacuum desiccator with $\sim 20 \mu\text{L}$ of 1H, 1H, 2H, and 2H-perfluorodecyltrimethoxysilane added in the bottom of the desiccator. Then, the desiccator was evacuated to $\sim 10 \text{ mbar}$. The reaction lasted for 12 h. Finally, the substrates were heated in an oven at 120°C for 2 h before further experiments were undertaken.

The measurements were conducted using a contact angle goniometer (OCA35, Dataphysics). Advancing and receding contact angles were determined by increasing and decreasing the droplet volume between 10 and $20 \mu\text{L}$ at the rate of $1 \mu\text{L s}^{-1}$. Sliding angles were determined with a tilt speed of 1° s^{-1} . The videos and contact angles were recorded continuously by a commercially available program (SCA). The sliding velocities of liquid droplets on tilted PDMS brushes were determined from the corresponding videos. Each result was repeated more than three times.

Condensation experiments were conducted in a well-sealed chamber with a vapor inlet and outlet (Figure 2a). The test sample was attached to a copper plate with thermally conductive paste (OMEGA, OT-201-2). Saturated vapor was controlled by a mass flow controller (OMEGA, FMA-A2208, $0\text{--}5 \text{ L min}^{-1}$). The chamber was filled with nitrogen before injecting the desired vapor. After the chamber was filled with vapor for 10 min, the surface was cooled down by a Peltier element until a specific subcooling was reached ($\sim 10 \text{ K}$). The surface temperature was measured by a thermistor. Videos were recorded using a camera (Ueye, UI-2240SE-C-HQ) attached to a microscope. Droplet characteristics were analyzed from recorded videos with Image J.

For measurements of coalescence time, the chamber was placed vertically. A high-speed camera (Photron, FASTCAM Mini UX100) was used to record the video at 4000 fps for image analysis.

Condensation heat transfer measurements were conducted in a custom-made setup, which consisted of a vapor generator, a condensation chamber, a chiller for cooling the substrate, a vacuum pump with a cold trap, and a camera. The vapor generator was heated by a heat plate. A magnetron in liquids ensured a well-mixed ethanol-water mixture. Temperature (OMEGA, PT100) and pressure (Vacuum Gauges, Pfeiffer, CCR362) inside the condensation chamber were measured in real-time throughout the measurement.

Condensing surfaces were mounted via thermally conductive paste (OMEGA, OT-201-2) on a copper plate vertically placed in the condensation chamber. Two thermistors (OMEGA, PT100) attached to the condensing surface were utilized to measure the

temperature of the substrate. A chilled water bath (Julabo, F25) was used to dissipate the heat from the condensing surface. A flow meter (MPM, FT-210) was used to measure the speed of the cooling water, and two thermistors (OMEGA, PT100) were used to measure the temperature of the inlet and outlet of the water. All these data were monitored and recorded by a data acquisition system in a LabVIEW program. A vacuum pump (Vacuumbrand, RC5 Chemistry Hybrid Vacuum Pump) was integrated to pump down the experimental system to vacuum conditions ($P_v < 10$ Pa) before the condensation chamber was filled with the desired vapor. Then, the condensation chamber was degassed more than three times. The liquids in the vapor generator were boiled for more than 30 min to remove the noncondensable gas before conducting the experiments. A camera (Sony Alpha 7 R III) was used to monitor the characteristics of droplets on surfaces during heat transfer measurements.

ACKNOWLEDGMENTS

This study was funded by the European Research Council (ERC) under the European Union's Horizon 2020 research and innovation program (grant agreement No 883631). Y. H. gratefully acknowledges the Alexander von Humboldt Foundation for financial support. J. L. gratefully acknowledges the National Natural Science Foundation of China for financial support. S.L. gratefully acknowledges China Scholarship Council (CSC) for his scholarship.

CONFLICT OF INTEREST

The authors declare no conflict of interest.

ORCID

Hans-Jürgen Butt  <http://orcid.org/0000-0001-5391-2618>

REFERENCES

- Shi S, Cui X, Han H, Weng J, Li Z. A study of the heat transfer performance of a pulsating heat pipe with ethanol-based mixtures. *Appl Therm Eng*. 2016;102:1219-1227.
- Su Q, Chang S, Song M, Zhao Y, Dang C. An experimental study on the heat transfer performance of a loop heat pipe system with ethanol-water mixture as working fluid for aircraft anti-icing. *Int J Heat Mass Transf*. 2019;139:280-292.
- Rabbi KF, Ho JY, Yan X, et al. Polydimethylsiloxane-silane synergy enables dropwise condensation of low surface tension liquids. *Adv Funct Mater*. 2022;32(19):2112837.
- Wang T, Sheng C, Nnanna AGA. Experimental investigation of air conditioning system using evaporative cooling condenser. *Energy Build*. 2014;81:435-443.
- Jin H, Lin G, Bai L, Zeiny A, Wen D. Steam generation in a nanoparticle-based solar receiver. *Nano Energy*. 2016;28:397-406.
- Donati M, Lam CWE, Milionis A, et al. Sprayable thin and robust carbon nanofiber composite coating for extreme jumping dropwise condensation performance. *Adv Mater Interfaces*. 2020;8(1):2001176.
- Sharma CS, Stamatopoulos C, Suter R, von Rohr PR, Poulikakos D. Rationally 3d-textured copper surfaces for laplace pressure imbalance-induced enhancement in dropwise condensation. *ACS Appl Mater Interfaces*. 2018;10(34):29127-29135.
- Chen X, Wu J, Ma R, et al. Nanograsped micropyrnidal architectures for continuous dropwise condensation. *Adv Funct Mater*. 2011;21(24):4617-4623.
- Cho HJ, Preston DJ, Zhu Y, Wang EN. Nanoengineered materials for liquid-vapour phase-change heat transfer. *Nat Rev Mater*. 2017;2:16092.
- Wen R, Ma X, Lee Y, Yang R. Liquid-vapor phase-change heat transfer on functionalized nanowired surfaces and beyond. *Joule*. 2018;2(11):2307-2347.
- Zhang N. Innovative heat pipe systems using a new working fluid. *Int Commun Heat Mass Transf*. 2001;28(8):1025-1033.
- Taft BS, Williams AD, Drolen BL. Review of pulsating heat pipe working fluid selection. *J Thermophys Heat Transf*. 2012;26(4):651-656.
- Srimuang W, Amatachaya P. A review of the applications of heat pipe heat exchangers for heat recovery. *Renew Sust Energ Rev*. 2012;16(6):4303-4315.
- Rettig A, Lagler M, Lamare T, et al. Presented at world engineers' convention. Geneva; 2011.
- Lion S, Michos CN, Vlaskos I, Rouaud C, Taccani R. A review of waste heat recovery and organic rankine cycles (ORC) in on-off highway vehicle heavy duty diesel engine applications. *Renew Sust Energ Rev*. 2017;79:691-708.
- Hung TC, Shai TY, Wang SK. A review of organic rankine cycles (ORCs) for the recovery of low-grade waste heat. *Energy*. 1997;22(7):661-667.
- Preston DJ, Lu Z, Song Y, et al. Heat transfer enhancement during water and hydrocarbon condensation on lubricant infused surfaces. *Sci Rep*. 2018;8:540.
- Xiao R, Miljkovic N, Enright R, Wang EN. Immersion condensation on oil-infused heterogeneous surfaces for enhanced heat transfer. *Sci Rep*. 2013;3:1988.
- Sett S, Sokalski P, Boyina K, et al. Stable dropwise condensation of ethanol and hexane on rationally designed ultrascale nanostructured lubricant-infused surfaces. *Nano Lett*. 2019;19:5287-5296.
- Khalil K, Soto D, Farnham T, et al. Grafted nanofilms promote dropwise condensation of low-surface-tension fluids for high-performance heat exchangers. *Joule*. 2019;3:1377-1388.
- Rykaczewski K, Paxson AT, Staymates M, et al. Dropwise condensation of low surface tension fluids on omniphobic surfaces. *Sci Rep*. 2014;4:4158.
- Liu J, Sun Y, Zhou X, et al. One-step synthesis of a durable and liquid-repellent poly(dimethylsiloxane) coating. *Adv Mater*. 2021;33(23):2100237.
- Wyslouzil BE, Wolk J. Overview: Homogeneous nucleation from the vapor phase-the experimental science. *J Chem Phys*. 2016;145(21):211702.
- Turnbull D. Kinetics of heterogeneous nucleation. *J Chem Phys*. 1950;18:198-203.
- Hou Y, Butt HJ, Kappl M. Water and ice nucleation on solid surfaces. In: Mittal KL, Choi CH, eds. *Ice Adhesion: Mechanism, Measurement and Mitigation*. John Wiley & Sons; 2020:55-86.
- Wang L, McCarthy TJ. Covalently attached liquids: Instant omniphobic surfaces with unprecedented repellency. *Angew Chem Int Ed Engl*. 2016;55(1):244-248.
- Woo S, Vollmer D. Silicone brushes: Omniphobic surfaces with low sliding angles. *Angew Chem Int Ed Engl*. 2016;55(24):6822-6824.
- Buddingh JV, Hozumi A, Liu G. Liquid and liquid-like surfaces/coatings that readily slide fluids. *Prog Polym Sci*. 2021;123:101468.
- Gao N, Geyer F, Pilat DW, et al. How drops start sliding over solid surfaces. *Nat Phys*. 2018;14:191-196.
- Extrand CW, Gent AN. Retention of liquid drops by solid surfaces. *J Colloid Interface Sci*. 1990;138(2):431-442.

31. Brown RA, Orr FM, Scriven LE. Static drop on an inclined plate: Analysis by the finite element method. *J Colloid Interface Sci.* 1980;73(1):76-87.
32. Cha H, Vahabi H, Wu A, et al. Dropwise condensation on solid hydrophilic surfaces. *Sci Adv.* 2020;6(2):eaax0746.
33. Cheng Y, Wang M, Sun J, et al. Rapid and persistent suction condensation on hydrophilic surfaces for high-efficiency water collection. *Nano Lett.* 2021;21(17):7411-7418.
34. Hou Y, Yu M, Chen X, Wang Z, Yao S. Recurrent filmwise and dropwise condensation on a beetle mimetic surface. *ACS Nano.* 2015;9(1):71-87.
35. Beysens D, Knobler CM. Growth of breath figures. *Phys Rev Lett.* 1986;57(12):1433-1436.
36. Sharma CS, Combe J, Giger M, Emmerich T, Poulikakos D. Growth rates and spontaneous navigation of condensate droplets through randomly structured textures. *ACS Nano.* 2017;11(2):1673-1682.
37. Boreyko JB, Chen C-H. Self-propelled dropwise condensate on superhydrophobic surfaces. *Phys Rev Lett.* 2009;103(18):184501.
38. Miljkovic N, Enright R, Wang EN. Effect of droplet morphology on growth dynamics and heat transfer during condensation on superhydrophobic nanostructured surfaces. *ACS Nano.* 2012;6(2):1776-1785.
39. Miljkovic N, Enright R, Nam Y, et al. Jumping-droplet-enhanced condensation on scalable superhydrophobic nanostructured surfaces. *Nano Lett.* 2013;13(1):179-187.
40. Wen R, Xu S, Ma X, Lee Y-C, Yang R. Three-dimensional superhydrophobic nanowire networks for enhancing condensation heat transfer. *Joule.* 2018;2(2):269-279.
41. Wen R, Li Q, Wu J, et al. Hydrophobic copper nanowires for enhancing condensation heat transfer. *Nano Energy.* 2017;33:177-183.
42. Wen R, Xu S, Zhao D, et al. Sustaining enhanced condensation on hierarchical mesh-covered surfaces. *Natl Sci Rev.* 2018;5(6):878-887.
43. Stylianou SA, Rose JW. Drop-to-filmwise condensation transition: Heat transfer measurements for ethanediol. *Int J Heat Mass Transf.* 1983;26(5):747-760.
44. Rose JW. On the mechanism of dropwise condensation. *Int J Heat Mass Transf.* 1967;10(6):755-762.
45. Narhe R, Beysens D, Nikolayev VS. Contact line dynamics in drop coalescence and spreading. *Langmuir.* 2004;20(4):1213-1221.
46. Kapur N, Gaskell PH. Morphology and dynamics of droplet coalescence on a surface. *Phys Rev E.* 2007;75:056315.
47. Eddi A, Winkels KG, Snoeijer JH. Influence of droplet geometry on the coalescence of low viscosity drops. *Phys Rev Lett.* 2013;111(14):144502.
48. Sharma CS, Lam CWE, Milionis A, Eghlidi H, Poulikakos D. Self-sustained cascading coalescence in surface condensation. *ACS Appl Mater Interfaces.* 2019;11(30):27435-27442.
49. Chu F, Yan X, Miljkovic N. How superhydrophobic grooves drive single-droplet jumping. *Langmuir.* 2022;38(14):4452-4460.
50. Zhao G, Zou G, Wang W, et al. Competing effects between condensation and self-removal of water droplets determine anti-frosting performance of superhydrophobic surfaces. *ACS Appl Mater Interfaces.* 2020;12(6):7805-7814.
51. Liu C, Zhao M, Zheng Y, Lu D, Song L. Enhancement and guidance of coalescence-induced jumping of droplets on superhydrophobic surfaces with a U-groove. *ACS Appl Mater Interfaces.* 2021;13(27):32542-32554.
52. Lo CW, Chu YC, Yen MH, Lu MC. Enhancing condensation heat transfer on three-dimensional hybrid surfaces. *Joule.* 2019;3(11):2806-2823.
53. Ma J, Sett S, Cha H, Yan X, Miljkovic N. Recent developments, challenges, and pathways to stable dropwise condensation: A perspective. *Appl Phys Lett.* 2020;116:260501.

SUPPORTING INFORMATION

Additional supporting information can be found online in the Supporting Information section at the end of this article.

How to cite this article: Li S, Diaz D, Kappl M, Butt H-J, Liu J, Hou Y. Enhanced condensation heat transfer by water/ethanol binary liquids on polydimethylsiloxane brushes. *Droplet.* 2022;1:214-222. doi:10.1002/dro2.31